PNAS RESEARCH ARTICLE | CELL BIOLOGY

WNK1 collaborates with TGF-β in endothelial cell junction turnover and angiogenesis

Ankita B. Jaykumar[a], Sakina Plumber[a,1], David M. Barry[b], Derk Binns[a], Chonlarat Wichaidit[a], Magdalena Grzemska[a], Svetlana Earnest[a], Elizabeth J. Goldsmith[c], Ondine Cleaver[b], and Melanie H. Cobb[a,2]

Contributed by Melanie H. Cobb; received March 2, 2022; accepted May 2, 2022; reviewed by Shmuel Muallem and Christopher Hughes

Angiogenesis is essential for growth of new blood vessels, remodeling existing vessels, and repair of damaged vessels, and these require reorganization of endothelial cell–cell junctions through a partial endothelial–mesenchymal transition. Homozygous disruption of the gene encoding the protein kinase WNK1 results in lethality in mice near embryonic day (E) 12 due to impaired angiogenesis. This angiogenesis defect can be rescued by endothelial-specific expression of an activated form of the WNK1 substrate kinase OSR1. We show that inhibition of WNK1 kinase activity not only prevents sprouting of endothelial cells from aortic slices but also vessel extension in inhibitor-treated embryos ex vivo. Mutations affecting TGF-β signaling also result in abnormal vascular development beginning by E10 and, ultimately, embryonic lethality. Previously, we demonstrated cross-talk of WNK1 with TGF-β–regulated SMAD signaling, and OSR1 was identified as a component of the TGF-β interactome. However, molecular events jointly regulated by TGF-β and WNK1/OSR1 have not been delineated. Here, we show that inhibition of WNK1 promotes TGF-β–dependent degradation of the tyrosine kinase receptor AXL, which is involved in TGF-β–mediated cell migration and angiogenesis. We also show that interaction between OSR1 and occludin, a protein associated with endothelial tight junctions, is an essential step to enable tight junction turnover. Furthermore, we show that these phenomena are WNK1 dependent, and sensitive to TGF-β. These findings demonstrate intimate connections between WNK1/OSR1 and multiple TGF-β–sensitive molecules controlling angiogenesis and suggest that WNK1 may modulate many TGF-β–regulated functions.

WNK1 | TGF-β | OSR1 | EndMT | occludin

Significance

Deletion of WNK1 in mice causes embryonic lethality due to failed vascular development. WNK1 is best known for its importance in blood pressure control; mutations in the gene can lead to Gordon's syndrome. Much of WNK1 signaling is mediated by downstream protein kinases OSR1 (oxidative stress responsive 1) and SPAK (STE20/SPS1-related proline-, alanine-rich kinase). This study characterizes an essential contribution of WNK1 in angiogenesis by influencing processes regulated by transforming growth factor-β (TGF-β) and presents a mechanism of tight junction and adherens junction turnover through interaction with OSR1. Collaborations between WNK1/OSR1 and TGF-β mediators are identified that fine tune essential processes in angiogenesis and may contribute to context-specificity in TGF-β signaling, with implications in development, wound repair, and cancer biology.

Angiogenesis is a highly regulated process which is turned on transiently during development, reproduction, and wound repair, which involves formation of new capillaries by sprouting or by splitting off from the original vessel (intussuception) (1, 2). Homozygous disruption of the gene encoding the protein kinase with no lysine (K) 1 (WNK1) results in a lethal developmental failure in mice around embryonic day (E) 12, due to impaired angiogenesis (3, 4). WNK1 is the most ubiquitously expressed of a family of four related, multifunctional, and atypical protein-serine/threonine kinases, notable for their unique catalytic lysine location (5). WNK1 phosphorylates substrates, the best characterized of which are oxidative stress-responsive 1 (OSR1) and STE20/SPS-1–related proline-alanine–rich kinase (SPAK, *STK39*), critical for maintaining cellular ion homeostasis (5–9). The phenotype of the WNK1 global knockout mouse mimics the defects caused by endothelial-specific ablation of WNK1 and is rescued either by endothelial-specific expression of WNK1 (3) or an activated form of OSR1 (4). Additionally, depletion of WNK1 and OSR1 decreased in vitro vascular cord formation and cell migration in endothelial cells (10), indicating a crucial role of WNK1-activated OSR1 signaling in angiogenesis, cell migration, and vascular remodeling.

Recently, we identified the transcription factor Slug (*SNAI2*) in WNK1-mediated control of cell migration and vascular network formation (10). Slug is a master regulator of endothelial–mesenchymal transition (Endo-MT) and is important in regulating angiogenic sprouting (11, 12). Partial Endo-MT is characterized by transient loss of an endothelial phenotype and acquisition of mesenchymal characteristics such as loss of cell–cell junctions, polarity, and gain of motility to promote angiogenic sprouting and cell migration (2, 10–19). During vein-graft remodeling, Slug mediates mesenchymal transition via the SMAD2/3 axis–mediated transforming growth factor-β (TGF-β) signaling (11, 17), a widely known inducer of mesenchymal transition (20, 21). We previously showed that WNK1 interacts with and phosphorylates SMAD2 and regulates its function (15, 22). We thus hypothesized that WNK1 signaling takes part in the regulation of TGF-β/SMAD–dependent Endo-MT for promoting onset of cell sprouting, migration, and vascular remodeling.

Reviewers: S.M., Instituto Nacional de Saude; and C.C.H., University of California, Irvine.

The authors declare a competing interest. O.C. published a review article with one of the referees in 2018 (https://link.springer.com/article/10.1007/s10456-018-9613-x).

[1]Present address: Columbia University Graduate School of Arts and Sciences, New York, NY 10027

[2]To whom correspondence may be addressed. Email: Melanie.Cobb@UTSouthwestern.edu.

This article contains supporting information online at http://www.pnas.org/lookup/suppl/doi:10.1073/pnas.2203743119/-/DCSupplemental.

Published July 22, 2022.

Phenotypic plasticity in several cancers is dependent on the expression of the receptor tyrosine kinase AXL. In normal mammary epithelial cells, AXL was also shown to be a driver of stemness (23, 24). Of note, WNK1 was identified as a signature gene in breast cancer initiation by transposon insertional mutagenesis in mice (25). We observed a connection between WNK1 and AXL in breast cancer cells (26). Interestingly, several characteristics of epithelial–mesenchymal transition overlap with those in endothelial cells (19). Endothelial-expressed AXL is known to modulate angiogenesis (27–29). The catalytic activity of AXL induces endothelial tube formation in vitro, and knockdown of AXL in breast cancer cells and in endothelial cell coculture impairs this process (28, 29). AXL was identified as a downstream effector of TGF-β and modulates expression of TGF-β/SMAD–dependent target genes involved in cell migration in hepatocellular carcinoma (30–32). Moreover, inhibition of AXL decreases autocrine TGF-β signaling in hepatocellular carcinoma and impairs secretion of proangiogenic factors in breast cancer cells, which, in turn, affects the function of endothelial cells in coculture and in vivo (30, 33). Paracrine angiogenic factors have also been shown to be expressed in endothelial cells, suggestive of an autocrine signaling loop (34). In view of these observations, we investigated the potential of an AXL and WNK1 signaling collaboration in endothelial cells to regulate endothelial cell migration and tube formation.

Mesenchymal transition involves loss of a fraction of cell–cell contacts. TGF-β initiates cytoskeletal turnover and a drastic down-regulation and disintegration of tight junctions to promote migration in endothelial cells (35, 36). Upon TGF-β stimulation, the TGF-β receptor type II redistributes into tight junctions, which leads to dissolution of tight junctions (37, 38). Occludin also localizes to endothelial tight junctions. While occludin is not necessary for the formation of tight junctions, occludin is vital in regulating tight junction integrity (37, 38). Occludin is likewise important for directional migration of epithelial cells (39). Furthermore, recent studies have shown that occludin is also involved in endothelial neovascularization and angiogenesis (40).

Adherens junctions are required for endothelial cell stabilization and homeostasis because they promote contact inhibition of growth and decrease cell responsiveness to apoptotic stimuli. Adherens junctions in endothelial cells primarily consist of VE-cadherin (41, 42). VE-cadherin is also known to be an endothelial cell–specific regulator of TGF-β/SMAD signaling (41). TGF-β induces TGF-βRII association with VE-cadherin, and this clustering promotes TGF-β signaling, which, in turn, destabilizes cell–cell junctions (43). Moreover, VE-cadherin is essential for TGF-β–induced endothelial cell migration (41).

In this study, we identify multiple molecular events that underlie WNK1-mediated control of angiogenesis and endothelial motility. We show that WNK1 is required for maintaining expression of the tyrosine kinase receptor AXL, which is involved in promoting secretion of angiogenic factors. In addition, we also demonstrate regulation of several TGF-β1 signaling mediators by WNK1. We show that interaction between OSR1 and occludin is an essential step to regulate tight junctions and angiogenesis in a WNK1-dependent manner.

Results

WNK Activity Is Required in the Endothelium for Angiogenesis. Global or endothelial-specific deletion of the *WNK1* gene in mice results in death by ∼E12 due to failed vascular development (3, 44). In mice, mutations affecting TGF-β signaling result in abnormal vascular development between E8 and E10 and, ultimately, embryonic lethality (45). Previous studies show that WNK1 knockout or depletion blocks angiogenesis during development and in cell-culture models in vitro (10) (*SI Appendix*, Fig. S1*A*). WNK inhibitors have been shown to interfere with cell migration but have not been reported in angiogenesis assays, to our knowledge (28). Here, we tested the efficacy of WNK inhibitors in blocking angiogenesis in multiple systems. Similar to WNK1 depletion, the WNK inhibitor WNK463 reduced cord formation in primary human umbilical vein endothelial cells (HUVECs), indicating that the kinase activity of WNK1 is required for angiogenesis (Fig. 1*A* and *B*). This inhibitor was shown to have high selectivity for WNKs, with remarkably little detectable inhibition of a panel of more than 400 other protein kinases (46). Real-time imaging of cord formation showed that primary HUVECs treated with WNK463 exhibited defects in cell migration, which is essential to angiogenesis (10) (*SI Appendix*, Movies S1 and S2).

Inhibition of endothelial cord formation was also observed in cells exposed to the WNK inhibitor SW133708 (Fig. 1*A* and *B*). SW133708 was identified in a screen for WNK1 inhibitors in the UT Southwestern High Throughput Screening Core (26). We next tested whether inhibition of WNK1 using SW133708 inhibited angiogenesis in mouse embryos between E8 and E10, during which time key angiogenic events occur, including development of intersomitic blood vessels (47). Intersomitic vessels are among the first vessels in the embryo to form by sprouting angiogenesis from preexisting blood vessels (47). Staining of mouse embryos with the endothelial marker PECAM showed that whole-embryo ex vivo treatment with the WNK1 inhibitor on ∼E9.0 decreased the length of intersomitic vessels (Fig. 1*C* and *D*). This provides evidence that WNK1 activity is involved in sprouting angiogenesis during embryonic blood-vessel development. We then tested whether WNK1 is involved in processes underlying postnatal sprouting angiogenesis, using mouse aortic-ring explants. We found that WNK463 suppressed sprouting of endothelial cords from the aorta and decreased the length of the cords emerging from the aortic explants (Fig. 1*E*–*G* and *SI Appendix*, Fig. S1*B*). These observations further support the conclusion that WNK1 activity is involved in angiogenesis (Fig. 1*H*).

Angiogenesis defects in WNK1-null mice are rescued by endothelial-specific expression of OSR1 (4). Consistent with this observation, we found that depletion of OSR1 also attenuated cord formation in primary HUVECs (10) (*SI Appendix*, Fig. S1*A*). Among the best validated targets of OSR1 are the sodium–potassium–2 chloride cotransporters, NKCC1 and NKCC2, that regulate ion balance and cell volume (48). NKCC1 is broadly expressed in tissues, including endothelial cells, and inhibition of NKCC1 activity is implicated in suppressing tumor angiogenesis (49). NKCCs are inhibited by furosemide-related diuretics such as bumetanide. We compared effects of bumetanide with WNK463 and observed that bumetanide inhibited cord formation of primary HUVECs but not nearly as effectively as WNK463 (Fig. 1*A* and *B*). These findings suggest that OSR1 is a significant mediator of WNK1-dependent angiogenesis; however, NKCC1 is only one of multiple inputs that contribute to WNK1-dependent angiogenesis downstream of OSR1.

WNK1 Stabilizes the TGF-β–Sensitive Angiogenic Tyrosine Kinase AXL. We previously showed the involvement of Slug in WNK1-mediated cell migration (10). Slug is transcriptionally activated by AXL in a feed-forward manner via TGF-β signaling as well as through SMAD3 (10, 50). AXL was shown to promote migration and partial mesenchymal transition in addition to being

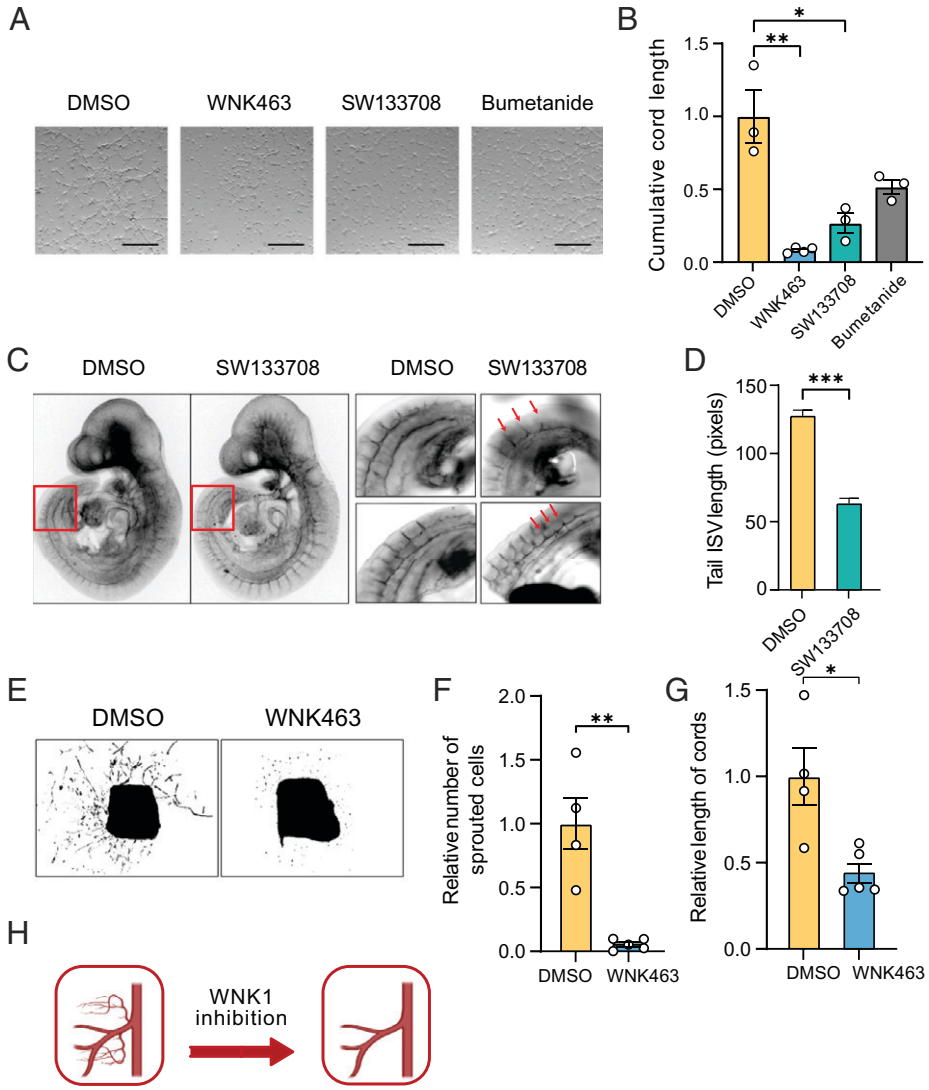

Fig. 1. WNK activity is required in the endothelium for angiogenesis. (*A*) Representative bright-field images of cord formation in HUVECs treated with DMSO, WNK463 (1 μM), SW113708 (10 μM), or bumetanide (20 μM); Scale bar, 1 mm. (*B*) Corresponding quantification of the images in *A* shows decreased length of cords in HUVECs treated with WNK463 or SW113708 for 4 to 6 h compared with DMSO control; $n = 3$. Only partial decrease in the cord length was seen with bumetanide treatment (20 μM). (*C*) Representative confocal images show PECAM staining in embryos treated with SW113708 (10 μM) or DMSO control applied to E9.25 embryos for 6 h in a BTC Precision chamber. (*D*) Corresponding quantification shows reduced length of intersomitic vessels (ISV) with SW113708 treatment compared with DMSO control; $n = 4$ ($n = 29$ images with DMSO; $n = 58$ images with SW133708). (*E*) Simulated bright-field images show sprouting cord formation by day 6 of DMSO and WNK463 (1 μM) treatment of mouse aortic ring slices. (*F*) Corresponding quantification shows decrease in the number of sprouted cells and (*G*) relative length of cords from the aortic explants in WNK463 treatment compared with DMSO control; $n = 5$. (*H*) Model depicting reduced angiogenesis upon WNK1 inhibition. Graphics created with BioRender.com. Data are represented as mean ± SE, analyzed by unpaired two-tailed Student's *t* test or one-way ANOVA. $^*P < 0.05$, $^{**}P < 0.005$, $^{***}P < 0.0005$.

involved in angiogenesis (28, 29). Thus, we examined the possible regulation of AXL by WNK1. Depletion of WNK1 using a previously validated WNK1 small interfering RNA (siRNA) (10, 51) decreased AXL protein expression (Fig. 2*A*). Similarly, we found that inhibition of WNK using WNK463 or SW133708 decreased AXL expression in human dermal microvascular endothelial cells (HDMECs) or HUVECs, respectively (Fig. 2*B*–*D*). However, knockdown of OSR1 had no effect on AXL in endothelial cells (see Fig. 4*E*).

In contrast to the full-length protein, the amount of the cleaved AXL fragment was unchanged by WNK inhibition (Fig. 2*E* and *F*). However, in the presence of WNK463, treatment with the proteasomal inhibitor MG132 decreased expression of AXL but increased accumulation of the cleaved AXL fragment (Fig. 2*E* and *F*). These findings suggest that inhibition or depletion of WNK1 increases cleavage of full-length AXL, which then undergoes proteasomal degradation. Supporting the hypothesis that WNK1 acts on AXL stability rather than biosynthesis, we found that WNK463 does not affect AXL mRNA in HUVECs (Fig. 2*G*). We then tested whether TGF-β signaling cooperates with WNK1 in mediating AXL turnover. Treatment with the TGF-β receptor inhibitor galunisertib in non–serum-starved conditions increased AXL expression, and cotreatment with WNK463 prevented this increase (Fig. 2*E* and *H*). These data suggest cooperation between WNK1 and TGF-β pathway components in mediating decreases in AXL expression. Because AXL signaling regulates endothelial permeability (22, 24), we propose that the control of AXL protein by WNK1 contributes to multistep regulation of endothelial tight junction integrity required during angiogenesis and vascular remodeling in a TGF-β–dependent manner.

Knockdown of AXL is known to reduce endothelial autocrine secretion of proangiogenesis factors mediated by the TGF-β pathway (30). Therefore, we asked whether inhibition

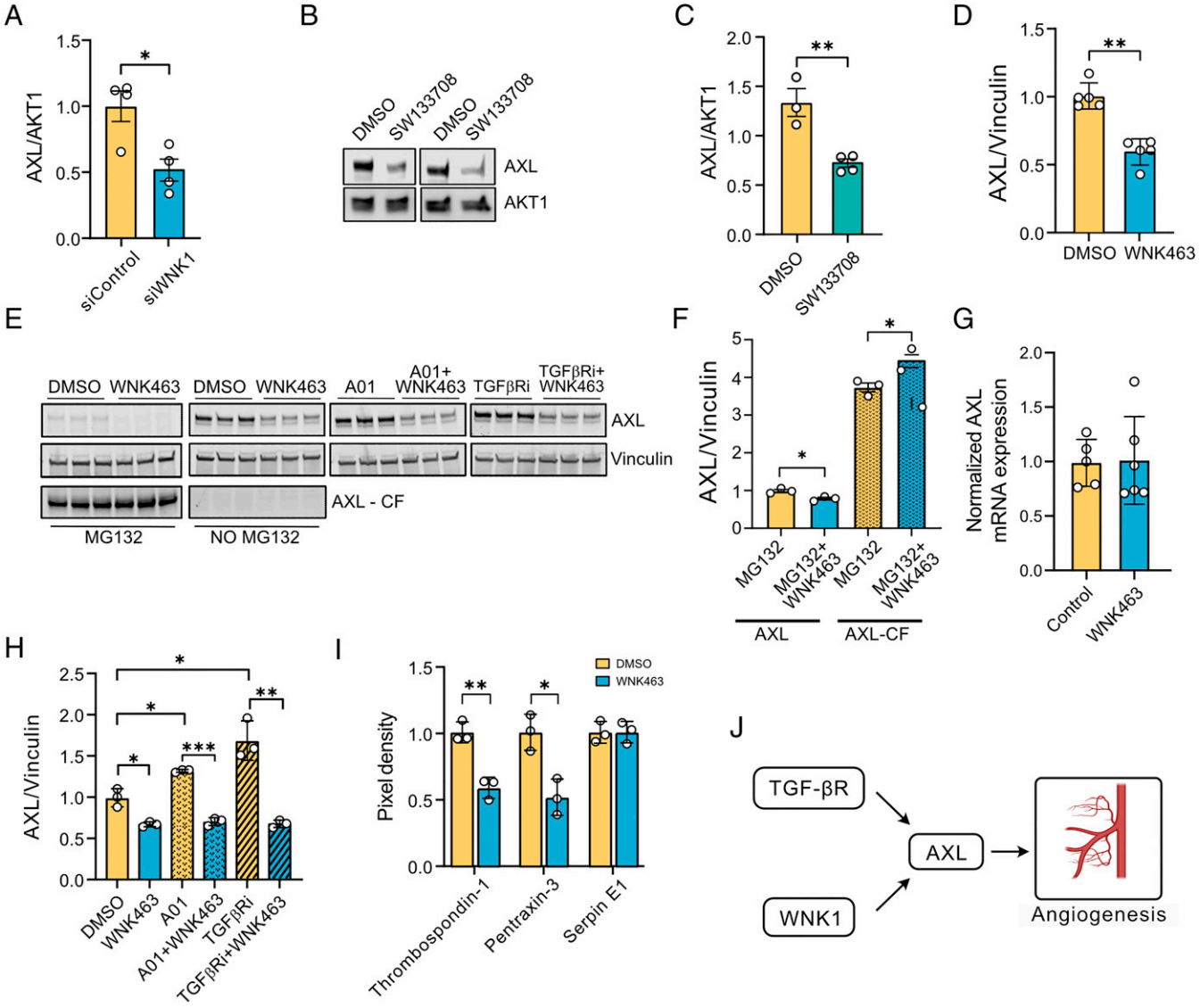

Fig. 2. WNK1 stabilizes the TGF-β–sensitive angiogenic tyrosine kinase AXL. (*A*) Western blot quantification shows decreased AXL expression upon WNK1 siRNA (control siRNA) depletion or siControl in HUVECs; $n = 4$. (*B*) Representative Western blots show AXL expression in cells treated with SW113708 (10 μM) overnight. (*C*) Corresponding quantification of the Western blots in *B* shows decreased AXL expression upon SW113708 treatment compared with DMSO control in HUVECs; $n = 4$. (*D*) Western blot quantification shows decreased AXL expression upon overnight WNK463 treatment compared with DMSO control in HDMECs; $n = 5$. (*E, Left*) Representative Western blot shows full-length and cleaved fragment of AXL upon treatment with DMSO control or the proteasomal inhibitor MG132 (10 μM) with or without WNK463 (1 μM) cotreatment in HUVECs. (*Right*) Representative Western blots show AXL expression in HUVECs treated with DMSO control or WNK463 (1μM) overnight and co-treatment with or without the SMURF1 inhibitor A01 (2μM) or TGFβ receptor inhibitor (TGFBRi: galunisertib, 1μM). (*F*) Corresponding quantification of *Left* panels in *E* shows increased accumulation of cleaved fragment of AXL upon WNK463+MG132 treatment compared with MG132 alone; $n = 3$. (*G*) Quantification of 18S normalized relative mRNA expression in HUVECs shows no change in mRNA expression of AXL treated with WNK463 compared with DMSO control; $n = 6$. (*H*) Corresponding quantification of *Right* panels in *E* show differences in AXL expression in cells treated with A01+WNK463 compared to A01 alone; $n = 3$. (*I*) Quantification of angiogenic factors secreted into conditional medium 4 h after initiation of cord formation in HUVECs treated with DMSO control or WNK463 (1 μM); $n = 3$. (*J*) Model figure shows the collaboration among WNK1 and TGF-β signaling in regulating AXL. Graphics were created with BioRender.com. Data are represented as mean ± SE analyzed by unpaired two-tailed Student's *t* test or one-way ANOVA. $^{*}P < 0.05$, $^{**}P < 0.005$, $^{***}P < 0.0005$.

of WNK leads to changes in secretion of angiogenesis factors from endothelial cells. Primary HUVECs were serum starved and the supernatants were collected during cord formation assays in cells treated with either DMSO or WNK463. We measured angiogenic factors secreted into the conditioned medium, using an angiogenesis array. We found that the secretion of thrombospondin-1 and pentraxin-3 was decreased in the conditioned medium collected from endothelial cells treated with WNK463, compared with the control, suggestive of autocrine signaling of these angiogenic factors, as has been previously reported (52, 53) (Fig. 2*I*). TGF-β1 decreases pentraxin-3 expression in a SMAD2/3–dependent manner (54), consistent with a TGF-β–mediated regulation of AXL by WNK1 (Fig. 2*J*).

WNK1 Enhances Stability of TGF-β–Dependent Factors. Given the intersection of TGF-β1 signaling and WNK1 signaling pathways, we tested if inhibition of WNK1 regulates other TGF-β1–sensitive components in endothelial cells. First, we tested whether WNK1 regulated SMAD2/3. We found that inhibition as well as knockdown of WNK1, using a previously validated WNK1 siRNA (10, 51), decreased SMAD2/3 in a

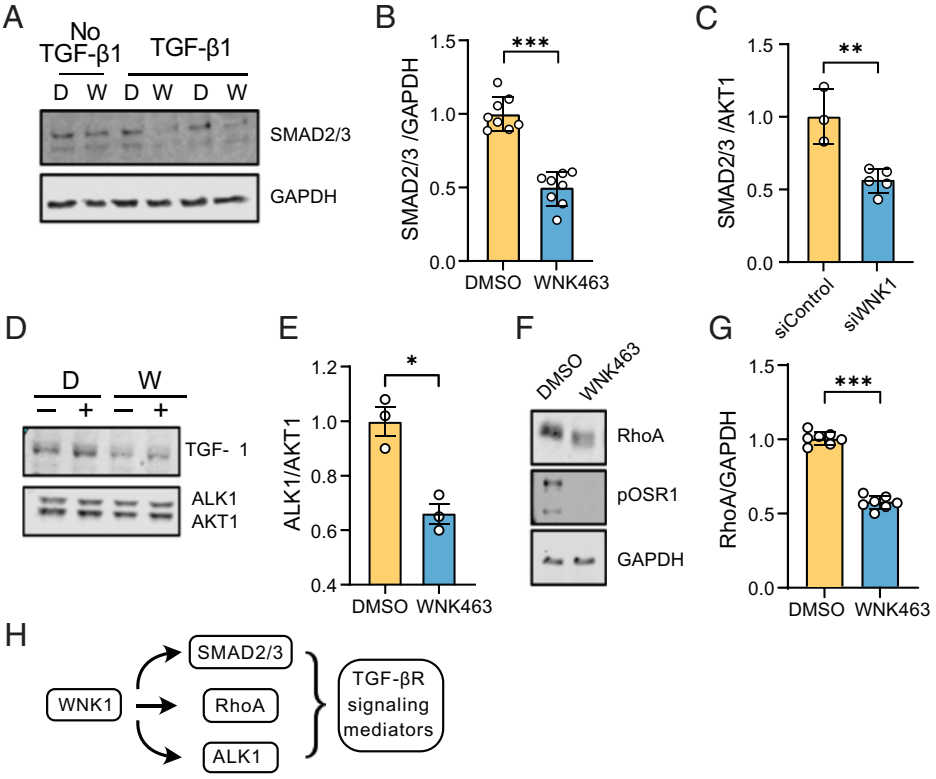

Fig. 3. WNK1 enhances stability of TGF-β–dependent factors. (*A*) Representative Western blots of SMAD2/3 expression upon overnight treatment with WNK463 (1 μM). (*B*) Corresponding quantification of images in *A* shows decreased SMAD2/3 expression in HUVECs treated with WNK463 compared with DMSO control; $n = 8$. (*C*) Quantification of SMAD2/3 expression in HDMECs treated with siWNK1 ($n = 5$) compared with siControl (control siRNA) ($n = 3$), (*D*) Representative Western blots of ALK1 expression in HUVECs treated with WNK463 compared with DMSO control cotreated with or without TGF-β1 (10 ng/mL). D, DMSO; W, WNK463. (*E*) Corresponding quantification of images in *D*; $n = 3$. (*F*) Representative Western blot of total RhoA expression in HUVECs treated with WNK463 compared with DMSO control. (*G*) Corresponding quantification of the Western blot in *F*; $n = 7$. (*H*) Model depicting regulation of TGF-β signaling mediators by WNK1. Data are represented as mean ± SE analyzed by unpaired two-tailed Student's *t* test. $^*P < 0.05$, $^{**}P < 0.005$, $^{***}P < 0.0005$.

TGF-β1–dependent manner (Fig. 3*A*–*C*), consistent with our previous findings in HeLa cells (15). We also found that inhibition as well as knockdown of WNK1 decreased ALK1, the endothelial-enriched TGF-β receptor type I in a TGF-β1–dependent manner (Fig. 3*D* and *E*). Non–SMAD-dependent signaling pathways are involved in regulation of Rho-like GTPase signaling pathways such as RhoA (55). Decreasing RhoA in endothelial cells suppresses angiogenesis (50). Therefore, we asked whether WNK1 regulates RhoA and found that inhibition of WNK1 decreases total RhoA (Fig. 3*F* and *G*). These results suggest that WNK1/OSR1 affect TGF-β signaling output via regulation of several TGF-β signaling mediators (Fig. 3*H*).

WNK1/OSR1 Collaborate with TGF-β to Regulate Tight Junction Turnover and Localization and Function of Occludin. TGF-β1 differentially regulates RhoA, leads to a decrease in total RhoA, and causes disintegration of tight junctions (36). TGF-β–dependent regulation of this process involves molecular mediators such as the GTPase CDC42 and its target kinase PAK1, and controlled clearance of endothelial tight junctions is an important step during vascular remodeling (36, 40, 56–59). We previously showed that OSR1 phosphorylates PAK1, which prevents its activation by CDC42 (60). In addition, OSR1 was found to be a component of the TGF-β interactome (35). Because OSR1 is one of the mediators of WNK1 action, we explored the possibility that WNK1 regulates OSR1 to influence endothelial tight junction turnover.

Occludin localizes to endothelial tight junctions. Although not necessary for the formation of tight junctions, occludin regulates tight junction integrity (37, 38). Therefore, we first tested whether occludin in HUVECs colocalized with OSR1. We found that colocalization between OSR1 and occludin was enhanced upon TGF-β1 treatment compared with that in the untreated condition, as indicated by the increase in Pearson's correlation coefficient (Fig. 4*A* and *B*). Next, we asked whether TGF-β1 affected activation of OSR1. We found that TGF-β1 partially reduced phosphorylation of OSR1 on an activating site, Ser325. When these cells were exposed to the WNK inhibitor WNK463, it effectively inactivated OSR1 as expected (Fig. 4*C* and *D*). These results indicate a collaboration among TGF-β and WNK signaling pathways in regulating occludin.

The association between OSR1 and occludin provoked us to ask how WNK1/OSR1 regulates occludin function. We found that depletion of OSR1 decreased occludin but not AXL protein in HDMECs (Fig. 4*E* and *F*). In addition, we found that inhibition of OSR1 activity by inhibiting WNK1 with WNK463 also decreased occludin protein in primary HUVECs (Fig. 4*G* and *H*). A comparable decrease in occludin protein amount was observed in WNK463-treated cells in which protein synthesis was suppressed with cycloheximide (*SI Appendix*, Fig. S2). In addition, we found no differences in occludin mRNA expression upon siRNA-mediated depletion of OSR1 (Fig. 4*I*). These findings suggest that the decrease in occludin protein expression upon WNK inhibition is not due to differences in transcription or translation of occludin mRNA; instead, the decrease suggests an effect on occludin stability.

Next, we tested whether OSR1 phosphorylates occludin and found that occludin immunoprecipitated from HUVECs was

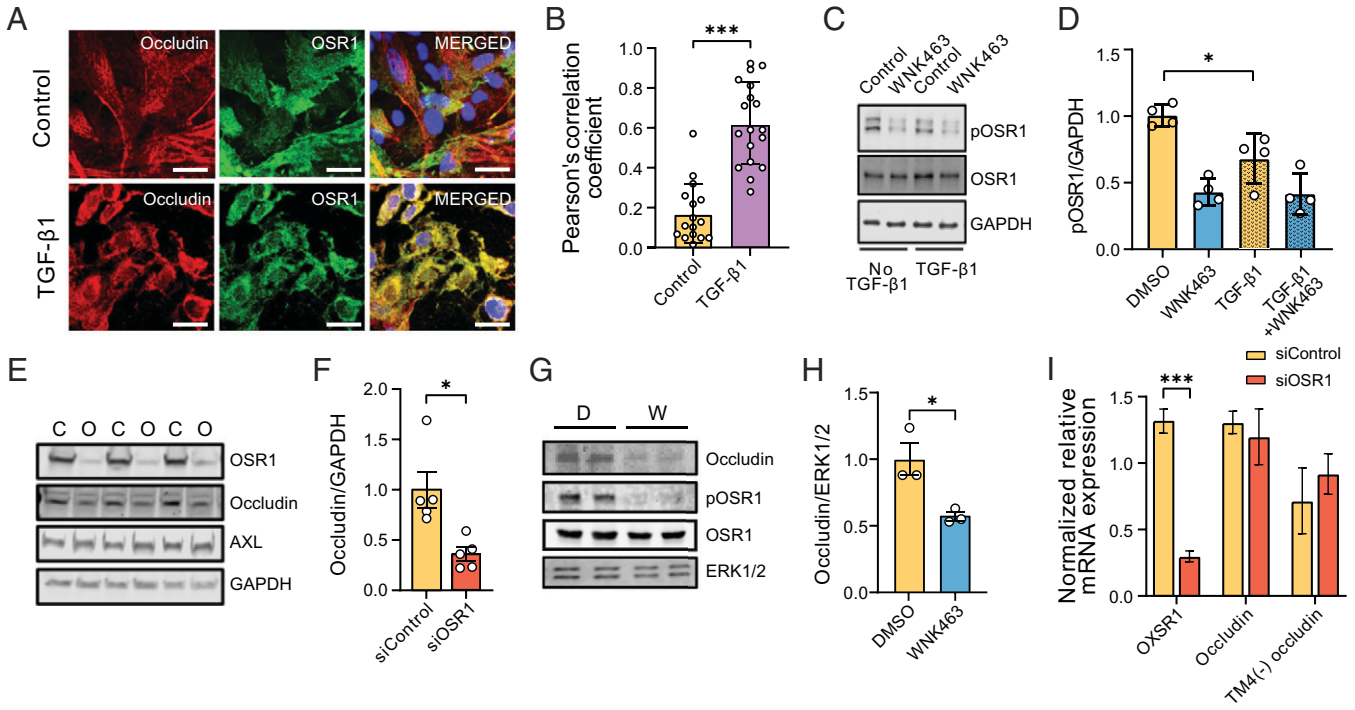

Fig. 4. WNK1/OSR1 collaborate with TGF-β to regulate tight junction turnover and localization and function of occludin. (*A*) Representative confocal images of immuno-fluorescently labeled endogenous occludin (red), OSR1 (green), and nucleus (DAPI: blue) in primary HUVECs with or without TGF-β1 (10 ng/mL) stimulation (no TGF-β1, $n = 16$; TGF-β1, $n = 18$). Merged panel (yellow) shows colocalization between occludin and OSR1. Scale bar, 20 μm. (*B*) Corresponding quantification of images in *A* colocalizing pixels was done by measuring Pearson's correlation coefficient shows increased colocalization with TGF-β1 treatment. (*C*) Representative Western blots show expression of phosphorylated Ser325 OSR1 in HUVECs treated with WNK463 (1 μM) and/or TGF-β1 (1 ng/mL). (*D*) Corresponding quantification of images in *C* shows decreased phosphorylated OSR1 (pOSR1) upon TGF-β1 treatment; $n = 4$. (*E*) Representative Western blots of occludin protein levels upon OSR1 knockdown in HDMECs. C, control siRNA; O, OSR1 siRNA. (*F*) Corresponding quantification of images in *E* shows decreased occludin expression 72 h after siOSR1 treatment compared with siControl (control siRNA), $n = 5$. (*G*) Representative Western blots show occludin protein levels treated with WNK463 compared with DMSO control. D, DMSO; W, WNK463. (*H*) Corresponding quantification of Western blots in *G* shows decreased occludin amount in WNK463-treated condition compared with DMSO control in HUVECs; $n = 3$. (*I*) Quantification of 18S-normalized relative mRNA expression in HDMECs shows no change in mRNA expression of occludin or TM-4(−) occludin (occludin isoform lacking fourth transmembrane domain) treated with siOSR1 compared with siControl; $n = 5$. Data are represented as mean ± SE analyzed by unpaired two-tailed Student's *t* test or one-way ANOVA. $^*P < 0.05$, $^{***}P < 0.0005$.

not phosphorylated by constitutively active OSR1 in vitro (*SI Appendix*, Fig. S3). These observations indicate WNK1-dependent OSR1 function regulates occludin by controlling its protein turnover but apparently not by directly phosphorylating it.

The C-Terminal Domain of OSR1 Interacts with Occludin to Influence Tight Junction Turnover. Given the colocalization of OSR1 with occludin (Fig. 4*A* and *B*), we asked whether colocalization indicated a stable association between the two proteins. Under control conditions, we saw no detectable endogenous coimmunoprecipitation of the two proteins; however, treatment with TGF-β1 caused a modest but detectable immunoprecipitation of OSR1 with occludin, consistent with their colocalization in TGF-β1–stimulated cells. Their association was strongly enhanced in cells exposed only to the WNK inhibitor WNK463 (Fig. 5*A*), which effectively inactivates OSR1 (46). In primary HUVECs, this association was lost in the presence of both TGF-β1 and the WNK inhibitor (Fig. 5*A*). Similarly, OSR1 colocalization with occludin, quantified by Pearson's correlation coefficient, was higher in the presence of WNK463 compared with control conditions (*SI Appendix*, Fig. S4). As noted, TGF-β1 partially reduced phosphorylation of OSR1 on an activating site, Ser325 (Fig. 4*C* and *D*), but it is unlikely that only inactive OSR1 associates with occludin, because this association was lost in the presence of both TGF-β1 and WNK463.

Structure–function analysis of the carboxyl-terminal (CCT) domain of OSR1 showed that it is a docking domain for proteins that contain R-F-x-V/I and/or a variant motif, R-x-F-x-V/I, forming a basis for its substrate recognition (61–63). Therefore, we evaluated whether the interaction of OSR1 with occludin could be mediated by this type of docking motif. To test this possibility, we coincubated the occludin immunoprecipitates from primary HUVECs with the peptide SAGRRFIVSPVPE that is capable of blocking the interaction between the OSR1 CCT and motif-containing proteins (62). We found that the amount of OSR1 coprecipitating with occludin was diminished in the presence of the blocking peptide (Fig. 5*B* and *C*). In human embryonic kidney (HEK293) cells overexpressing FLAG-occludin, we found a similar decrease in the amount of endogenous OSR1 coimmunoprecipitating with occludin in the presence of the blocking peptide (Fig. 5*D*). In addition, we found that overexpressed FLAG-occludin coimmunoprecipitated with myc-CCT-OSR1 (Fig. 5*E*). These observations suggest that occludin interacts with the C-terminal region of OSR1.

WNK1 Influences VE-Cadherin Expression in a TGF-β–Dependent Manner. The adherens junction protein VE-cadherin is an endothelial cell–specific regulator of TGF-β/SMAD signaling (41). TGF-β induces TGF-βRII association with VE-cadherin; this clustering promotes TGF-β signaling, and VE-cadherin is essential for TGF-β–induced endothelial cell migration (41). Therefore, we investigated the effect of WNK1 inhibition on TGF-β–dependent regulation of VE-cadherin. We observed that inhibition of WNK1/OSR1 activity with WNK463 caused a decrease in VE-cadherin expression in a TGF-β1–dependent

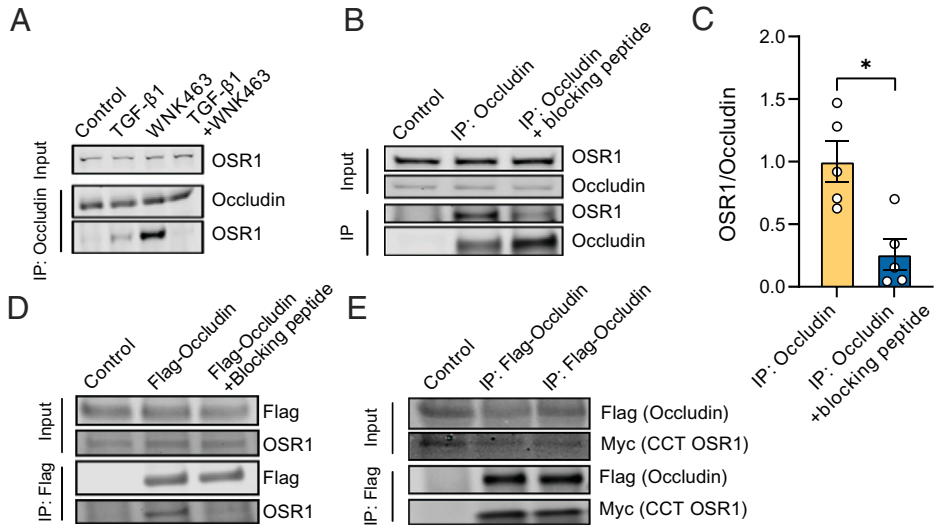

Fig. 5. The C-terminal domain of OSR1 interacts with occludin to influence tight junction turnover. (*A*) Representative Western blots show endogenous coimmunoprecipitation of OSR1 with occludin in primary HUVECs showing enhanced interaction of OSR1 and occludin upon overnight TGF-β (10 ng/mL) and WNK463 (1μM) treatment; $n = 5$. (*B*) Representative Western blots show endogenous coimmunoprecipitation of OSR1 and SMURF2 with occludin in HUVECs treated with WNK463 (1 μM) overnight, which is diminished upon coincubation with the blocking peptide SAGRRFIVSPVPE. (*C*) Corresponding quantification of OSR1 immunoprecipitated over occludin with or without the presence of blocking peptide; $n = 5$. (*D*) Representative Western blot show immunoprecipitation (IP) of FLAG-occludin overexpressed in HEK293 cells interacts with endogenous OSR1, which is blocked with coincubation with the blocking peptide SAGRRFIVSPVPE; $n = 5$. (*E*) Representative Western blots show immunoprecipitation of FLAG-occludin overexpressed in HEK293 cells and its interaction with myc-C-terminal OSR1.

manner (Fig. 6*A*–*D*). In addition, we found that treatment with WNK463 led to a decreased, continuous VE-cadherin staining pattern (suggestive of mature adherens junctions), consistent with a need for WNK1 to promote mature adherens junctions (Fig. 6*E* and *F*) (64). We also show that inhibition of WNK1 in HUVECs increases endothelial cell junction permeability using a Transwell assay (*SI Appendix*, Fig. S5*A*). Both findings suggest that inhibition of WNK1 negatively impacts the maturation of adherens junctions in endothelial cells. Together, these data suggest that WNK1/OSR1 can regulate the integrity of adherens junctions and their TGF-β–dependent actions.

Discussion

Our study shows that TGF-β signaling components such as the TGF-β receptor, RhoA, SMADs, occludin, VE-cadherin, and AXL are interconnected and act in a collaborative manner with WNK1/OSR1 signaling pathways (Fig. 6*G* and *SI Appendix*, Fig. S6*A*). This phenomenon may contribute, in part, to the context specificity in TGF-β signaling to influence endothelial remodeling.

Homozygous deletion of *WNK1* results in embryonic lethality in mice by ∼E12 as a result of defective angiogenesis and vascular development (3, 4). Here, we provide additional evidence that WNK1 is involved in sprouting angiogenesis during embryonic development as well as in postdevelopment conditions by utilizing both pre- and postnatal mouse explants. These findings suggest WNK1 is vital in mediating angiogenesis in both physiological (wound healing) and pathophysiological conditions (e.g., cancer). As a direct WNK1 substrate, OSR1 is one of the major mediators of WNK1 action, based on numerous lines of evidence. In addition, OSR1 was found to be a component of the TGF-β interactome (35). TGF-β1 regulates RhoA, leads to a decrease in total RhoA, and causes breakdown of the tight junctions (36). This process involves molecular mediators such as the GTPase CDC42 and its target kinase PAK1 for fine-tuned clearance of endothelial tight junctions, which is critical during vascular remodeling (36, 40, 56–59). We previously reported that OSR1 phosphorylates PAK1 and this prevents its activation by CDC42 (60). Because OSR1 is one of the known mediators of WNK1 action, we explored the possibility that WNK1 regulates OSR1 to influence endothelial tight junction turnover. We show that OSR1 is involved in WNK1-mediated regulation of turnover of tight junctions and adherens junctions, in part, through its interaction with occludin via a TGF-β–sensitive process. While occludin is not necessary for the formation of tight junctions, occludin is vital to tight junction integrity (37, 38). Interestingly, occludin is also important for directional migration of epithelial cells (39). Control of both tight junction integrity and directional migration of endothelial cells is central to angiogenesis (40, 47). One mechanism underlying the importance of WNK1/OSR1 to angiogenesis is the capacity to target occludin turnover. This same capacity may also contribute to effects of the WNK1 pathway on Endo-MT. We postulate that OSR1 interacts with and stabilizes occludin in endothelial tight junctions as loss of OSR1 depletes occludin, as does TGF-β1 signaling (36). Thus, WNK1/OSR1 is a critical mediator of TGF-β–dependent tight junction turnover. However, the mechanistic basis for the action of occludin in regulating tight junction turnover in endothelial cells is not known.

In this study, we show that full-length AXL is downregulated upon WNK1 inhibition. AXL signaling is regulated via its proteolysis-dependent degradation. One of the mechanisms involved in this process is presenilin-dependent, regulated, intramembrane, proteolysis-associated degradation. This occurs in two sequential steps: The first step is an ectodomain shedding, which is attributed to metalloproteases ADAM10 and tumor necrosis factor α–converting enzyme. The second step is an intramembrane cleavage by the γ-secretase complex, which includes presenilin enhancer 2 and presenilin 1 and 2, among others (65–67). This mechanism leads to the generation of a cleaved fragment of AXL corresponding to an ∼55 kDa band, which is rapidly removed through proteasomal degradation (66). In addition, inhibition of proteasomal activity accelerates

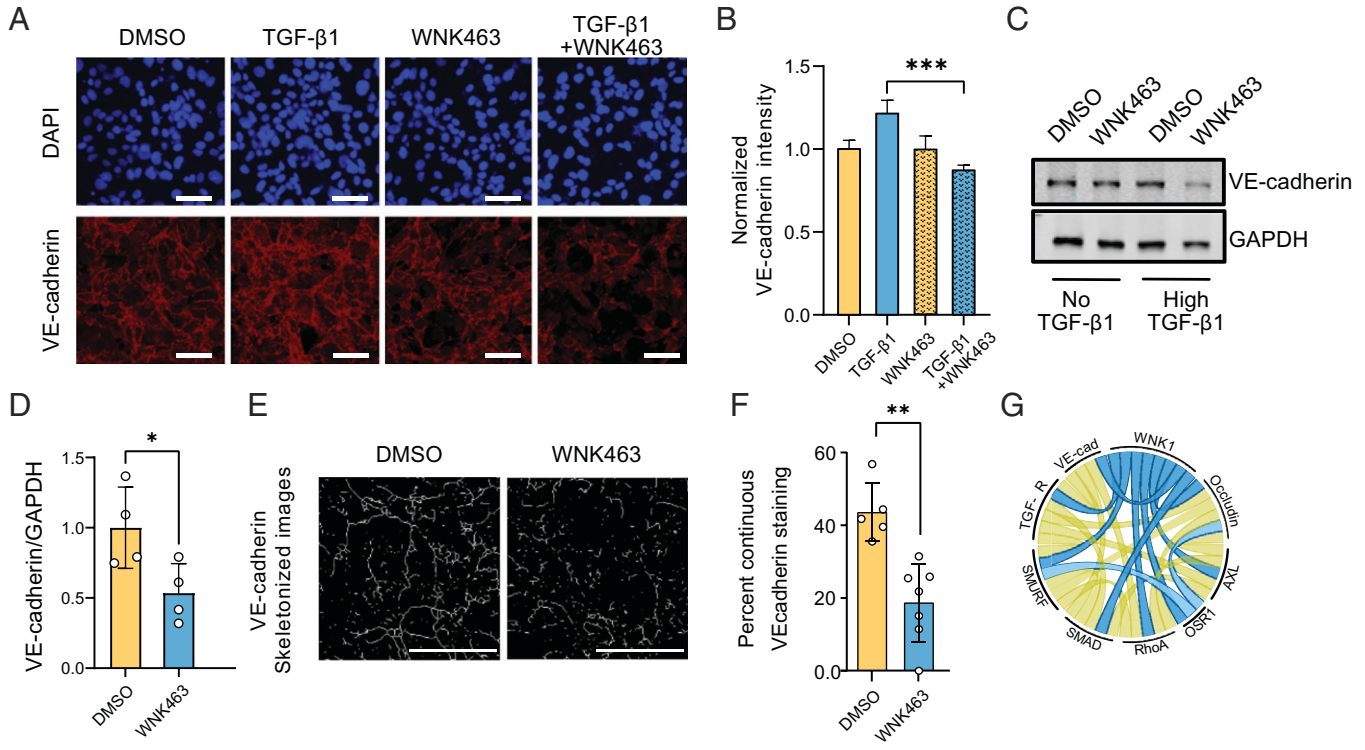

Fig. 6. WNK1 influences VE-cadherin expression in a TGF-β–dependent manner. (*A*) Representative confocal images of immuno-fluorescently labeled endogenous VE-cadherin (red) nucleus (DAPI: blue) in HDMECs with or without TGF-β1 (10 ng/mL) and/or WNK463 (1 μM) treatment. Scale bar, 60 μm. (*B*) Corresponding quantification shows decreased normalized fluorescence intensity of VE-cadherin in TGF-β1+WNK463 compared with TGF-β1 alone. DMSO: $n = 21$; WNK463: $n = 23$; TGF-β1: $n = 8$; and TGF-β1+WNK463: $n = 55$. (*C*) Representative Western blots show VE-cadherin expression upon overnight TGF-β1 (10 ng/mL) and/or WNK463 (1 μM) treatment in HUVECs. (*D*) Corresponding quantification of images in *C* shows decreased VE-cadherin expression in TGF-β1+WNK463 compared with TGF-β1 alone; $n = 4$. (*E*) Representative images showing "line structures" on VE-cadherin staining obtained from confocal images of HDMECs treated with DMSO or WNK463 (1 μM), both in the presence of TGF-β1 (10 ng/mL) using the MorphologicalSkeleton module. Scale bar, 35 μm. (*F*) Quantification of continuous VE-cadherin–staining pattern expressed as percentage of total VE-cadherin staining in HDMECs treated with DMSO or WNK463 (1 μM), both in the presence of TGF-β1 (10 ng/mL). Control: $n = 5$; WNK463: $n = 7$. (*G*) Chord diagram (80) depicting collaborative network among WNK1, OSR1, and TGF-β signaling mediators. Data are represented as mean ± SE analyzed by unpaired two-tailed Student's *t* test or one-way ANOVA. $*P < 0.05$, $**P < 0.005$, $***P < 0.0005$.

the proteolytic cleavage process of AXL, leading to reduced levels of full-length AXL in cells (67). This is consistent with our observations here, which suggest that inhibition of WNK1 leads to enhanced proteolytic cleavage of AXL.

AXL inhibition enhances the activity of proteolytic enzymes to promote cleavage of full-length AXL (67). In addition, WNK1 regulates the endothelial expression of metalloproteases MMP-2 and MMP-9 (10). Therefore, future studies will be needed to explore further mechanistic details of regulation of AXL and/or AXL-targeting proteolytic enzymes by WNK1. Stimulation of angiogenesis upon injury or by tumors occurs via secretion of proangiogenic factors (30). We previously showed that WNK1 promotes transcription of several angiogenic factors (10). Here, we further show that WNK1 also affects secretion of angiogenic factors into the conditioned media. Therefore, WNK1 may be involved in a concerted angiogenic response via regulating secretion of autocrine proangiogenic factors.

WNK is an atypical family of protein kinases due to the positioning of the ATP-binding, conserved lysine residue within the kinase domain (5). Of the 4 mammalian WNK isoforms, WNK1 is the most broadly expressed and the most highly expressed in endothelial cells, compared with other isoforms (10). WNK1 has been widely shown to regulate blood pressure in mice (8) and ion transport across cell membranes of several cell types (49). Mechanistically, WNK1 has been suggested to function as a chloride sensor through direct binding of a regulatory chloride ion in its active site, which inhibits its autophosphorylation (68). Recently, studies have proposed additional mechanisms underlying osmosensing by WNK1 through a conformational equilibrium between inactive, unphosphorylated, chloride-binding dimer and an autophosphorylation-competent monomer (69). Interestingly, osmotic pressure has also been shown to promote angiogenesis, three-dimensional migration, proliferation, and apoptosis in endothelial cells (55, 70). Recent studies show osmotic stress results in altered expression of TGF-β (71), altering TGF-β signaling. Therefore, we hypothesize that WNK1 may be a critical mediator of osmotic change-induced TGF-β signaling and angiogenesis.

VE-cadherin is a positive regulator of TGF-β–induced SMAD2/3 phosphorylation. TGF-β stimulation induces association of VE-cadherin with TGF-βRII/TGF-βRI and therefore it participates in maximal activation of the TGF-β pathway (41). A recent study showed that OSR1 phosphorylates the SMAD2/3 linker region to promote TGF-β signaling (22). Here, we found that WNK1 inhibition leads to decreased localization of VE-cadherin at cell–cell junctions only in the presence of TGF-β. Therefore, we hypothesize that WNK1/OSR1 signaling regulates VE-cadherin to affect TGF-β–dependent signaling output in a context-dependent manner.

Signal transduction pathways regulated by TGF-β control a diverse array of cellular processes, including embryogenesis, angiogenesis, proliferation, differentiation, migration, and apoptosis (45). Dysregulation of either ligands or mediators of this signaling pathway often cause disease or developmental defects (45).

Signaling specificity and versatility are present in the TGF-β signaling pathway and, importantly, it exhibits differential responses depending on the cellular context (45, 72, 73). This occurs through diverse regulatory mechanisms and cross-connections among SMAD-dependent and SMAD-independent, as well as TGF-β–dependent and TGF-β–independent, pathways (73, 74). The efficiency, amplitude, and duration of TGF-β signaling are tightly regulated by various mechanisms, including SMADs, proteasome-mediated degradation, phosphorylation by other protein kinase pathways, and subcellular localization, among others (73). These observations suggest that dynamic convergence of inputs via individual signaling nodes and subsequent modifications may fine tune TGF-β–SMAD signaling pathways to trigger diverse cellular outcomes. Consistent with this notion, our results suggest that WNK1 communicates with multiple nodes of the TGF-β signaling pathway and affects TGF-β signaling output in a context-dependent manner. In this study, we show that WNK1 collaborates with downstream TGF-β/SMAD signaling components including AXL, RhoA, ALK1, SMAD2/3, VE-cadherin, and occludin to regulate and fine tune essential processes in angiogenesis such as cell junction turnover in a context-dependent manner. Therefore, we propose that expression and activity of WNK1, and its ability to sense cell state (e.g., osmotic homeostasis and cell tension) may contribute, in part, to the context-specificity in TGF-β signaling.

Methods

Animals. All animal studies were performed according to UT Southwestern Medical Center (UTSW) Institutional Animal Care and Use Committee guidelines (animal protocol no. APN 2017–102338). WT Swiss Webster male mice were killed by decapitation, the thoracic/abdominal aorta was dissected, and the ex vivo explants were randomized for use in the aortic ring assay. Embryos at ∼E8.0 were obtained from gestating C57/BL6J mice and utilized in whole-embryo culture. Embryos were dissected and fixed in 4% paraformaldehyde (PFA)/phosphate-buffered saline (PBS) for 40 min at 4 °C, then dehydrated in 75% ethanol for storage at −20 °C (56).

Aortic Ring Assay. After dissecting the aorta, they were put in ice-cold PBS, and surrounding tissues were removed and cut in 1-mm pieces. Meanwhile, 48-well plates were coated with 150 μL of Cultrex RGF BME matrix type 2 (R&D Systems, 3533–005-02) or 200 μL of collagen type I (Fisher Scientific, CB354249). The plates were left to solidify the matrix for 30 min at 37 °C. Aortic rings were placed with tweezers in the middle of each well, incubated for 10 min, then covered with another 150 μL of Cultrex or collagen matrix, and incubated for 30 min at 37 °C. They were maintained for ∼13 to 18 d in culture and supplemented every 2 d with VascuLife media (Fisher Scientific, 50–311-891). Aortas were imaged every 2 d until the end of 18 d in culture. Interpretation of the assay was done using guidelines outlined in ref. 75. For analysis, we utilized ImageJ (76) to subtract image background, and we manually identified the sprouted cells, cords, and aortic rings. The regions of interest were then converted into binary masks. Subsequently, CellProfiler (77) was used to extract features (i.e., number of sprouted cells and cord lengths) from the masked images. Cord lengths were analyzed using the AnalyzeSkeleton tool in ImageJ.

Mouse Whole-Embryo Culture. The protocol was adapted from Dickinson and Lauderdale (78). Embryos were dissected with their yolk sac intact at E8.0 in Dulbecco's modified Eagle's medium (DMEM; Sigma-Aldrich, D5796) containing 8% fetal bovine serum (FBS; Sigma-Aldrich, F0926), and 1% penicillin-streptomycin (Thermo Fisher Scientific, SV30010)/antimycotic with HEPES. The embryos were cultured for 3 h in medium containing 50% male rat serum and 50% DMEM with HEPES and antibiotics in a Precision Incubator Unit (B.T.C. Engineering). WNK1 inhibitor (SW133708; 10 μM) or DMSO were all added in a randomized manner to the embryo culture for 6 h. After culture, whole-mount immunocytochemistry for PECAM and PECAM/endomucin costain was performed as previously described (78). After culture, embryos were imaged using a Zeiss Axio Observer epifluorescence microscope, then fixed at 4 °C with 4% PFA/PBS for 40 min.

Cell Lines. Primary human dermal microvascular endothelial cells (HMEC-1; ATCC, CRL-3243) were grown in complete MCDB medium (Fisher Scientific, MT15100CV) supplemented with 10% FBS (Sigma-Aldrich, F0926), 1% L-glutamine, 1% penicillin and streptomycin, 1 μg/mL hydrocortisone (Sigma Aldrich, H0888 or H6909), and 10 ng/mL epidermal growth factor (Cell Signaling Technology, 8916SC). HUVECs (ATCC, PCS-100-013) were grown in complete VascuLife EnGS media kit (Fisher Scientific, 50–311-891) supplemented per manufacturer's instructions. HEK293 cells were obtained from the Dr. Jenna Jewell laboratory (UTSW, Dallas, TX; cells purchased from ATCC, CRL-1573) and were grown in DMEM supplemented with 10% FBS and 1% penicillin-streptomycin. All the cells were maintained at 37 °C and 5% CO_2.

Constructs. Full-length human OSR1 (NM_005109) was excised from 3× FLAG CMV 7.1 (Sigma-Aldrich) with the restriction enzymes HindIII and BamHI. The resulting DNA fragment was ligated into the HindIII-BamHI digested vector CMV5m (N-terminally myc tagged CMV5). Clones were screened by HindIII-BamHI digests. Positive clones were verified by Sanger sequencing. OCLN (NCBI reference sequence: NM_002538.3) was ordered from the Ultimate ORF Lite human complementary DNA (cDNA) collection (Life Technologies) through the McDermott Center for Growth and Human Development at UTSW. OCLN was amplified by PCR with oligos incorporating a HindIII site at the N terminus and an XbaI site at the C terminus. The 1.6-kb OCLN PCR product was digested with HindIII-XbaI, purified, and ligated into the N-terminally tagged p3XFLAG-CMV-7.1 vector (Sigma) that had been digested with HindIII-XbaI.

In Vitro Endothelial Cord Formation Assay. Cord formation assay on Cultrex RGF BME matrix type 2 (Fisher Scientific, 35–330-1002) were performed as previously described (10). The cells were imaged with a Zeiss Axio Zoom V16 microscope (Carl Zeiss). Images were analyzed using the Image J software AnalyzeSkeleton tool. Analysis was performed in a blinded manner (to the identities of the images). For performing real-time imaging of cord formation, primary HUVEC cells were incubated with 1 μM Calcein AM dye (Fisher Scientific, 35–330-1002) for 20 min in complete medium. Stained cells were washed with PBS, trypsinized and plated at 10,000 cells/well of a 96-well plate (Greiner 655090) coated with 5 μL of Cultrex matrix, and incubated for 30 min at 37 °C before starting imaging. Wells were imaged using an IN Cell Analyzer 6000 automated microscope (GE Healthcare) with an environmentally controlled stage (37 °C and 5% CO_2) using a 10×/0.45 numeric aperture objective, 488-nm laser line, and fluorescein isothiocyanate emission filter. A single field at the center of each well was acquired every 3 min for 4 h.

Angiogenesis Array. Angiogenic factors secreted into conditioned media were measured using the Proteome Profiler Human Angiogenesis Array kit (R&D systems, ARY007), according to the manufacturer's instructions. The conditioned media used were from a cord formation assay in which 1×10^5 cells were seeded uniformly, and which had been pretreated with either DMSO or WNK463 overnight as well as during the cord formation assay. Briefly, the array blots were incubated with the conditioned media. After washing and incubating the blot with horseradish peroxidase (HRP)-conjugated secondary antibody, ChemiReagent Mix was used for chemiluminescent detection on X-ray film. The pixel density was analyzed using Image J software, and each pixel density was normalized to the corresponding pixel density of epidermal growth factor in each condition to normalize for the sample used for the array.

Coimmunoprecipitation. Cells were lysed in 1× lysis buffer (50 mM HEPES, 150 mM NaCl, 5 mM ethylenediaminetetraacetic acid [EDTA], 2% Triton X-100, 0.1% sodium dodecyl sulfate [SDS]) supplemented with protease inhibitor mixture, phenylmethylsulfonyl fluoride (PMSF), and phosphatase inhibitors (PhosStop; Sigma Aldrich, 4906837001). Cell extracts were harvested and cleared by centrifugation. We added to the cell lysate, in a 2:1 ratio, 1× immunoprecipitation (IP) buffer (50 mM HEPES, 100 mM NaCl, 5mM EDTA, and 1% 3-[(3-cholamidopropyl) dimethylammonio]-1-propanesulfonate [Sigma Aldrich, C3023]) supplemented with protease inhibitor mixture, PMSF, and phosphatase inhibitors (PhosStop; Sigma Aldrich, 4906837001). Samples were incubated with primary antibody (control sample incubated with rabbit immunoglobulin G primary

antibody) for 3 h at 4 °C and then with Protein A/G PLUS-Agarose beads (Santa Cruz Biotechnology, sc-2003) for 35 min with head-to-tail rotation. This was performed either in the absence or presence of CCT blocking peptide SAGRRFIVSPVPE (United Biosystems). Samples were then washed three times with 1× IP buffer before adding 6× SDS buffer (0.012% bromophenol blue, 30% glycerol, 10% SDS, 350 mM Tris-Cl, with 5% β-mercaptoethanol) and heating at 90 °C for 2 min. Samples were then resolved on 4% to 20% Mini-PROTEAN TGX Precast Protein Gels (Bio-Rad, 4568096) or 12% polyacrylamide gels before being transferred to polyvinylidene fluoride (PVDF) membranes. Membranes were then washed in tris-buffered saline plus Tween (TBS-T) before being blocked with TBS-based blocking buffer (LI-COR). Membranes were incubated with primary antibodies and then washed again before being incubated with species-specific, light chain–specific secondary antibodies (Jackson ImmunoResearch Labs, 115–655-174 and 211–622-171) and imaged using LI-COR imaging.

Immunofluorescence. HUVEC cells were fixed on glass coverslips (Fisher Scientific, 12–545-80) with 4% PFA for 20 min at room temperature. Coverslips were washed with sterile PBS and blocked in 10% normal goat serum (Life Technologies, 50–062Z) before incubating with primary antibodies for 1 h at room temperature. Coverslips were washed with 1× PBS. Subsequently, cells were incubated with an Alexa Fluor 488 conjugated goat–anti-mouse secondary antibody (Thermo Fisher Scientific, A11029) and Alexa Fluor 594 conjugated goat–anti-rabbit secondary antibody (Thermo Fisher Scientific, A11037) for 45 min at room temperature in dark, and the slides were mounted with DAPI Fluoromount-G (Thermo Fisher Scientific, 00–4959-52). Immunofluorescence images were acquired using a Zeiss LSM880 inverted confocal microscope (Carl Zeiss). Images were deconvolved using AutoQuant software (Media Cybernetics). The colocalizing pixels were identified and Pearson's correlation coefficient was determined using Imaris software (Oxford Instruments). For quantification shown in Fig. 6*B*, ImageJ (76) was used to subtract image background. Average intensity for each treatment was obtained using CellProfiler (77). CellProfiler (77) was used to enhance "line structures" on VE-cadherin images, segment the VE-cadherin objects, and skeletonize using the MorphologicalSkeleton module. Total object skeleton length for each frame was extracted at the end. The continuous VE-cadherin lengths, denoted as *skL*, equal or longer than the 90th percentile of the skeleton length distribution from the analysis of the DMSO condition, denoted as *skCL*, was used. The ratio of cumulative lengths, $\sum skCL$, to cumulative total skeleton length, $\sum skL$, per frame was calculated and is shown in Fig. 6*F*.

Transwell Permeability Assay. The Transwell permeability assay we used was modified from ref. 79. Primary HUVECs were seeded on a Transwell in a 24-well plate for 5 d. They were then incubated with either DMSO or WNK463 (1 μM) in both the upper and the lower compartments for 18 h. Then, 400 μL of serum-free medium was added to the lower compartment. A mixture of streptavidin-HRP, 15 μL, was added to 1 mL of serum-free medium and 200 μL of this mixture was added to the upper compartment and incubated for 15 min at 37 °C. Then 20 μL of the medium from the lower compartment was removed and added to a 96-well plate. To this, 50 μL of 1× 3,3′,5,5′-tetramethylbenzidine (TMB) substrate was added and incubated for 5 min. Then, 25 μL of 2N H_2SO_4 solution (i.e., stop solution) was added to stop the reaction, and absorption was measured at 450 nm using an enzyme-linked immunosorbent assay reader.

siRNA Knockdown. We utilized oligonucleotides encoding siRNA for human WNK1 (siWNK1: 5′ CAGACAGUGCAGUAUUCACTT 3′) and control siRNA (Thermo Fisher Scientific, 4390844), as in refs. 10 and 51, and OSR1 siRNA (Thermo Fisher Scientific, s19303 Silencer Select). HDMEC cells were transfected with 20 nM siRNA using Lipofectamine RNAiMax reagent (Invitrogen, 56532). After 24 to 72 h of transfection, cells were provided their respective treatments and were then harvested in 1× SDS buffer (0.002% bromophenol blue, 5% glycerol, 1.6% SDS, and 58 mM Tris-Cl) with 5% β-mercaptoethanol. The specificity of the WNK1 siRNA used in this manuscript has been validated in previous publications from our laboratory using as many as four independent siRNAs to target WNK1 (10, 51). The WNK1 siRNA with the highest efficacy was chosen for WNK1 knockdown experiments in this study, providing a complement to findings with WNK inhibitors.

Immunoblotting. Cell lysates containing 1× SDS buffer were homogenized with a 27-G syringe and whole lysates were run on 4% to 20% Mini-PROTEAN TGX Precast Protein Gels (Bio-Rad, 4568096) or 6/10/12% home-made polyacrylamide gels before being transferred to PVDF membranes (Bio-Rad, 1620177). Membranes were then washed in TBS-T before being blocked with TBS-based blocking buffer (LI-COR). Membranes were incubated with primary antibodies and then washed again before being incubated with species-specific secondary antibodies and imaged using LI-COR imaging.

Reverse Transcription and qPCR. RNA from HDMEC cells was extracted using PureLink RNA kit (Thermo Fisher Scientific, 12183018A). RNA concentration was measured and 1 μg was used to synthesize cDNA using iScript Reverse Transcription Supermix (Bio-Rad, 1708891) per manufacturer's instructions. The resultant cDNA was diluted 1:10 in nuclease-free water and the concentration was measured. The qPCR reactions with the cDNA and appropriate forward and reverse primers were set up using iTaq Universal SYBR Green Supermix (Bio-Rad, 1725121) per manufacturer's instructions. The qPCR cycle was as follows: 95 °C for 5 min, then 95 °C for 10 s, and 55 °C for 30 s for 40 cycles. Custom oligos were purchased from Thermo Fisher Scientific: OXSR1 (forward primer: AGGGACGATTACGAGCTGC; reverse primer: TCCGTTTGATTGCCACTTTCTC), occludin (forward primer: GGTCTAGGACGCAGCAGATTG; reverse primer: TGGACTTTCAAGAGGCCTGG), TM4 occludin (forward primer: TGGGAGTGAACCCAACTGCT; reverse primer: CTTCAGGAACCGGCGTGGAT), AXL (forward primer: GGTGGCTGTGAAGACGATGA; reverse primer: CTCAGATACTCCATGCCACT), and 18s (forward primer: GTAACCCGTTGAACCCCATT; reverse primer: CCATCCAATCGGTAGTAGCG).

Reagents. The following reagents, substrates, and plates were used: WNK463 (Selleck Chemicals, S8358); SMURF1 inhibitor A01 (Sigma Aldrich, SML1404); Galunisertib LY2157299 (Selleck Chemicals, S2230); MG132 (Sigma Aldrich, M7449); TGF-β1 (Cell Signaling Technology, 8915LC); anti–acetylated tubulin antibody (Sigma Aldrich, T7451); anti-Axl antibody C89E7 (Cell Signaling, 8661S); anti–vinculin antibody (Sigma Aldrich, V9131); anti–pOSR1 antibody (EMD Millipore, 07–2273); anti–OSR1 polyclonal antibody (Cell Signaling, 3729S); anti–OSR1 monoclonal antibody (VWR, 10624–616); anti–WNK1 antibody (Cell Signaling, 4979S); anti–occludin monoclonal antibody (Fisher Scientific, 33–150-0); anti–occludin polyclonal antibody (Thermo Fisher Scientific, 711500); anti–AKT1 antibody (Cell Signaling Technology, 2967L); anti–VE-cadherin antibody (Santa Cruz Biotechnology, sc-9989); anti–GAPDH antibody (Cell Signaling Technology, 97166L); anti–PECAM1 antibody (BD Biosciences, 553370); anti–myc antibody (Cell Signaling Technology, 2278S); anti–SMAD2/3 antibody (Millipore Sigma, 07–408); anti–ALK1 antibody (R&D Systems, AF370); anti–RhoA antibody (Santa Cruz Biotechnology, sc-418); anti–FLAG antibody (Sigma-Aldrich, F1804); Q256 WNK1 antibody was homemade as in ref. 1; Optimem (Invitrogen, 51985–034); Lipofectamine 2000 (Life Technologies, 11668019); bumetanide (Sigma Aldrich, B3023); 96-well plates (Corning, 3904; or Greiner, 655090); Corning 6.5 mm Transwell inserts with 0.4-μm polycarbonate membranes in a 24-well plate (Corning, 3413); streptavidin-HRP (R&D Systems, DY998); and TMB substrate (Sigma-Aldrich, T0440).

Statistics and Reproducibility. The data are presented as mean ± SEM from at least three independent experiments with similar results. All presented micrographs (immunofluorescence images) are representative images from three representative experiments as indicated in the figure legends. For the quantification of immunofluorescence images, the number of cells used for each representative experiment is indicated, and *P* values between two groups were determined using unpaired *t* tests. For results encompassing multiple groups, one-way ANOVA used the ANOVA command in SAS to determine the overall statistical outlook among the groups. Single intergroup comparisons between two groups were performed with two-tailed Student's *t* test as specifically mentioned in each case. Two-way ANOVA was used to determine differences between more than two treatments and groups. $P < 0.05$ was considered statistically significant.

Data Availability. We will follow all NIH policies with respect to sharing reagents, materials, and information with other investigators. Detailed protocols are provided to everyone who requests them. Upon publication, this manuscript will be submitted to the National Library of Medicine's PubMed Central as outlined by NIH policy. All study data are included in the article and/or supporting information.

ACKNOWLEDGMENTS. We thank the members of the M.H.C. laboratory and other contributing laboratories for valuable suggestions, and Dionne Ware for administrative assistance. We thank Steve Stippec (M.H.C. laboratory) for his help with molecular cloning of constructs used in this study. We also thank Dr. David Mangelsdorf (Department of Pharmacology, University of Texas Southwestern Medical Center, Dallas) for providing fresh mouse aortic slices. We thank Dr. Kate Luby-Phelps (Department of Cell Biology, University of Texas Southwestern Medical Center, Dallas) for consultation and advice on our confocal images. These studies were supported by NIH grant R01 HL147661 and Mary Kay Foundation grant 18-18 to M.H.C.; American Heart Association postdoctoral fellowship 18POST34030438 to A.B.J.; Cancer Prevention and Research Institute of Texas (CPRIT) training grant RP160157 for support of M.G. and early support of A.B.J.; Welch Foundation grants I11243 and I1128 to M.H.C. and E.J.G.; Cancer CPRIT grant RP190421 and NIH grant DK110358 to E.G.J.; and NIH grant HL126518 to O.C. Real-time imaging of cord formation was performed in collaboration with Dr. Hanspeter Niederstrasser (High-Throughput Screening Core, University of Texas Southwestern Medical Center). This work was also supported in part by an NIH-sponsored S10 grant (1S10OD018005-01 to Bruce A. Posner) for the IN Cell Analyzer 6000 and the Cancer Center P30 grant (3P30CA142543-10S3). The authors acknowledge the assistance of the UT Southwestern Live Cell Imaging Facility, a Shared Resource of the Harold C. Simmons Cancer Center, supported in part by the National Cancer Institute (Cancer Center support grant, 1P30 CA142543-01) and NIH Shared Instrumentation Award 1S10 OD021684-01 to Dr. Kate Luby-Phelps (LSM880 Airyscan).

Author affiliations: [a]Department of Pharmacology, UT Southwestern Medical Center, Dallas, TX 75390; [b]Department of Molecular Biology, UT Southwestern Medical Center, Dallas, TX 75390; and [c]Department of Molecular Biophysics, UT Southwestern Medical Center, Dallas, TX 75390

Author contributions: A.B.J., O.C., and M.H.C. designed research; A.B.J., S.P., D.M.B., D.B., M.G., and S.E. performed research; E.J.G. and O.C. contributed new reagents/analytic tools; A.B.J., D.M.B., D.B., C.W., M.G., and S.E. analyzed data; A.B.J. and M.H.C. wrote the paper; and O.C. edited the manuscript.

1. J. Folkman, Y. Shing, Angiogenesis. *J. Biol. Chem.* **267**, 10931–10934 (1992).
2. Z. K. Otrock, R. A. Mahfouz, J. A. Makarem, A. I. Shamseddine, Understanding the biology of angiogenesis: Review of the most important molecular mechanisms. *Blood Cells Mol. Dis.* **39**, 212–220 (2007).
3. J. Xie *et al.*, Endothelial-specific expression of WNK1 kinase is essential for angiogenesis and heart development in mice. *Am. J. Pathol.* **175**, 1315–1327 (2009).
4. J. Xie, J. Yoon, S. S. Yang, S.-H. Lin, C. L. Huang, WNK1 protein kinase regulates embryonic cardiovascular development through the OSR1 signaling cascade. *J. Biol. Chem.* **288**, 8566–8574 (2013).
5. B. Xu *et al.*, WNK1, a novel mammalian serine/threonine protein kinase lacking the catalytic lysine in subdomain II. *J. Biol. Chem.* **275**, 16795–16801 (2000).
6. J. A. McCormick, D. H. Ellison, The WNKs: Atypical protein kinases with pleiotropic actions. *Physiol. Rev.* **91**, 177–219 (2011).
7. F. H. Wilson *et al.*, Human hypertension caused by mutations in WNK kinases. *Science* **293**, 1107–1112 (2001).
8. A. C. Vitari, M. Deak, N. A. Morrice, D. R. Alessi, The WNK1 and WNK4 protein kinases that are mutated in Gordon's hypertension syndrome phosphorylate and activate SPAK and OSR1 protein kinases. *Biochem. J.* **391**, 17–24 (2005).
9. T. Moriguchi *et al.*, WNK1 regulates phosphorylation of cation-chloride-coupled cotransporters via the STE20-related kinases, SPAK and OSR1. *J. Biol. Chem.* **280**, 42685–42693 (2005).
10. H. A. Dbouk *et al.*, Actions of the protein kinase WNK1 on endothelial cells are differentially mediated by its substrate kinases OSR1 and SPAK. *Proc. Natl. Acad. Sci. U.S.A.* **111**, 15999–16004 (2014).
11. K. M. Welch-Reardon *et al.*, Angiogenic sprouting is regulated by endothelial cell expression of Slug. *J. Cell Sci.* **127**, 2017–2028 (2014).
12. M. M. Mahmoud *et al.*, Shear stress induces endothelial-to-mesenchymal transition via the transcription factor Snail. *Sci. Rep.* **7**, 3375 (2017).
13. S. Piera-Velazquez, S. A. Jimenez, Endothelial to mesenchymal transition: Role in physiology and in the pathogenesis of human diseases. *Physiol. Rev.* **99**, 1281–1324 (2019).
14. A. Nakao *et al.*, TGF-beta receptor-mediated signalling through Smad2, Smad3 and Smad4. *EMBO J.* **16**, 5353–5362 (1997).
15. B.-H. Lee, W. Chen, S. Stippec, M. H. Cobb, Biological cross-talk between WNK1 and the transforming growth factor β-Smad signaling pathway. *J. Biol. Chem.* **282**, 17985–17996 (2007).
16. N. R. Adams *et al.*, WNK lysine deficient protein kinase 1 regulates human endometrial stromal cell decidualization, proliferation, and migration in part through mitogen-activated protein kinase 7. *Biol. Reprod.* **97**, 400–412 (2017).
17. B. C. Cooley *et al.*, TGF-β signaling mediates endothelial-to-mesenchymal transition (EndMT) during vein graft remodeling. *Sci. Transl. Med.* **6**, 227ra34 (2014).
18. Y. Yoshimatsu, T. Watabe, Roles of TGF-β signals in endothelial-mesenchymal transition during cardiac fibrosis. *Int. J. Inflamm.* **2011**, 724080 (2011).
19. K. M. Welch-Reardon, N. Wu, C. C. Hughes, A role for partial endothelial-mesenchymal transitions in angiogenesis? *Arterioscler. Thromb. Vasc. Biol.* **35**, 303–308 (2015).
20. E. Pardali, G. Sanchez-Duffhues, M. C. Gomez-Puerto, P. Ten Dijke, TGF-β-induced endothelial-mesenchymal transition in fibrotic diseases. *Int. J. Mol. Sci.* **18**, 2157 (2017).
21. Y. Nakajima, T. Yamagishi, S. Hokari, H. Nakamura, Mechanisms involved in valvuloseptal endocardial cushion formation in early cardiogenesis: Roles of transforming growth factor (TGF)-beta and bone morphogenetic protein (BMP). *Anat. Rec.* **258**, 119–127 (2000).
22. Y. Li *et al.*, OSR1 phosphorylates the Smad2/3 linker region and induces TGF-β1 autocrine to promote EMT and metastasis in breast cancer. *Oncogene* **40**, 68–84 (2020).
23. A. S. T. Engelsen, K. Wnuk-Lipinska, S. Bougnaud, *et al.*, AXL is a driver of stemness in normal mammary gland and breast cancer. *iScience* **23**, 101649 (2020).
24. N. Fujino, H. Kubo, R. A. Maciewicz, Phenotypic screening identifies Axl kinase as a negative regulator of an alveolar epithelial cell phenotype. *Lab. Invest.* **97**, 1047–1062 (2017).
25. L. Chen *et al.*, Breast cancer transposon mutagenesis signature. *Proc. Natl. Acad. Sci. U.S.A.* **114**, E2215–E2224 (2017).
26. A. B. Jaykumar *et al.*, WNK1 enhances migration and invasion in breast cancer models. *Mol. Cancer Ther.* **20**, 1800–1808 (2021).
27. M. Gallicchio *et al.*, Inhibition of vascular endothelial growth factor receptor 2-mediated endothelial cell activation by Axl tyrosine kinase receptor. *Blood* **105**, 1970–1976 (2005).
28. Y. Li *et al.*, Axl as a potential therapeutic target in cancer: Role of Axl in tumor growth, metastasis and angiogenesis. *Oncogene* **28**, 3442–3455 (2009).
29. S. J. Holland *et al.*, Multiple roles for the receptor tyrosine kinase Axl in tumor formation. *Cancer Res.* **65**, 9294–9303 (2005).
30. P. Reichl *et al.*, Axl activates autocrine transforming growth factor-β signaling in hepatocellular carcinoma. *Hepatology* **61**, 930–941 (2015).
31. T. Bauer *et al.*, Identification of Axl as a downstream effector of TGF-β1 during Langerhans cell differentiation and epidermal homeostasis. *J. Exp. Med.* **209**, 2033–2047 (2012).
32. H. J. Lee, Y. M. Jeng, Y. L. Chen, L. Chung, R. H. Yuan, Gas6/Axl pathway promotes tumor invasion through the transcriptional activation of Slug in hepatocellular carcinoma. *Carcinogenesis* **35**, 769–775 (2014).
33. M. Tanaka, D. W. Siemann, Axl signaling is an important mediator of tumor angiogenesis. *Oncotarget* **10**, 2887–2898 (2019).
34. S. Lee *et al.*, Autocrine VEGF signaling is required for vascular homeostasis. *Cell* **130**, 691–703 (2007).
35. M. Barrios-Rodiles *et al.*, High-throughput mapping of a dynamic signaling network in mammalian cells. *Science* **307**, 1621–1625 (2005).
36. B. Ozdamar *et al.*, Regulation of the polarity protein Par6 by TGFbeta receptors controls epithelial cell plasticity. *Science* **307**, 1603–1609 (2005).
37. P. M. Cummins, Occludin: One protein, many forms. *Mol. Cell. Biol.* **32**, 242–250 (2012).
38. R. Rao, Occludin phosphorylation in regulation of epithelial tight junctions. *Ann. N. Y. Acad. Sci.* **1165**, 62–68 (2009).
39. D. Du *et al.*, The tight junction protein, occludin, regulates the directional migration of epithelial cells. *Dev. Cell* **18**, 52–63 (2010).
40. X. Liu *et al.*, Occludin S490 phosphorylation regulates vascular endothelial growth factor-induced retinal neovascularization. *Am. J. Pathol.* **186**, 2486–2499 (2016).
41. N. Rudini *et al.*, VE-cadherin is a critical endothelial regulator of TGF-beta signalling. *EMBO J.* **27**, 993–1004 (2008).
42. E. Dejana, Endothelial cell-cell junctions: Happy together. *Nat. Rev. Mol. Cell Biol.* **5**, 261–270 (2004).
43. J. Ma, G. Sanchez-Duffhues, M. J. Goumans, P. Ten Dijke, TGF-β–induced endothelial to mesenchymal transition in disease and tissue engineering. *Front. Cell Dev. Biol.* **8**, 260 (2020).
44. J. G. Lai *et al.*, Zebrafish WNK lysine deficient protein kinase 1 (wnk1) affects angiogenesis associated with VEGF signaling. *PLoS One* **9**, e106129 (2014).
45. F. Lebrin, M. Deckers, P. Bertolino, P. Ten Dijke, TGF-beta receptor function in the endothelium. *Cardiovasc. Res.* **65**, 599–608 (2005).
46. K. Yamada *et al.*, Small-molecule WNK inhibition regulates cardiovascular and renal function. *Nat. Chem. Biol.* **12**, 896–898 (2016).
47. J. R. Walls, L. Coultas, J. Rossant, R. M. Henkelman, Three-dimensional analysis of vascular development in the mouse embryo. *PLoS One* **3**, e2853 (2008).
48. W. L. Demian *et al.*, The ion transporter NKCC1 links cell volume to cell mass regulation by suppressing mTORC1. *Cell Rep.* **27**, 1886–1896.e6 (2019).
49. C. J. Heise *et al.*, Serum and glucocorticoid-induced kinase (SGK) 1 and the epithelial sodium channel are regulated by multiple with no lysine (WNK) family members. *J. Biol. Chem.* **285**, 25161–25167 (2010).
50. F. T. Zahra *et al.*, Endothelial RhoA GTPase is essential for in vitro endothelial functions but dispensable for physiological in vivo angiogenesis. *Sci. Rep.* **9**, 11666 (2019).
51. S. Gallolu Kankanamalage *et al.*, Multistep regulation of autophagy by WNK1. *Proc. Natl. Acad. Sci. U.S.A.* **113**, 14342–14347 (2016).
52. C. L. O'Neill *et al.*, Endothelial cell-derived pentraxin 3 limits the vasoreparative therapeutic potential of circulating angiogenic cells. *Cardiovasc. Res.* **112**, 677–688 (2016).
53. D. M. Smadja *et al.*, Thrombospondin-1 is a plasmatic marker of peripheral arterial disease that modulates endothelial progenitor cell angiogenic properties. *Arterioscler. Thromb. Vasc. Biol.* **31**, 551–559 (2011).
54. H. Li, H. M. Chang, Z. Shi, P. C. K. Leung, SNAIL mediates TGF-β1-induced downregulation of pentraxin 3 expression in human granulosa cells. *Endocrinology* **159**, 1644–1657 (2018).
55. D. Yoshino *et al.*, Hydrostatic pressure promotes endothelial tube formation through aquaporin 1 and Ras-ERK signaling. *Commun. Biol.* **3**, 152 (2020).
56. D. M. Barry *et al.*, Rasip1-mediated rho GTPase signaling regulates blood vessel tubulogenesis via nonmuscle Myosin II. *Circ. Res.* **119**, 810–826 (2016).
57. S. Terry, M. Nie, K. Matter, M. S. Balda, Rho signaling and tight junction functions. *Physiology (Bethesda)* **25**, 16–26 (2010).
58. V. Wong, Phosphorylation of occludin correlates with occludin localization and function at the tight junction. *Am. J. Physiol.* **273**, C1859–C1867 (1997).
59. T. Murakami, E. A. Felinski, D. A. Antonetti, Occludin phosphorylation and ubiquitination regulate tight junction trafficking and vascular endothelial growth factor-induced permeability. *J. Biol. Chem.* **284**, 21036–21046 (2009).
60. W. Chen, M. Yazicioglu, M. H. Cobb, Characterization of OSR1, a member of the mammalian Ste20p/germinal center kinase subfamily. *J. Biol. Chem.* **279**, 11129–11136 (2004).
61. K. Piechotta, N. Garbarini, R. England, E. Delpire, Characterization of the interaction of the stress kinase SPAK with the Na+-K+-2Cl- cotransporter in the nervous system: Evidence for a scaffolding role of the kinase. *J. Biol. Chem.* **278**, 52848–52856 (2003).

62. C. A. Taylor, 4th *et al.*, OSR1 regulates a subset of inward rectifier potassium channels via a binding motif variant. *Proc. Natl. Acad. Sci. U.S.A.* **115**, 3840–3845 (2018).
63. F. Villa *et al.*, Structural insights into the recognition of substrates and activators by the OSR1 kinase. *EMBO Rep.* **8**, 839–845 (2007).
64. K. M. Gray, D. B. Katz, E. G. Brown, K. M. Stroka, Quantitative phenotyping of cell-cell junctions to evaluate ZO-1 presentation in brain endothelial cells. *Ann. Biomed. Eng.* **47**, 1675–1687 (2019).
65. J. Ni *et al.*, Gas6 attenuates sepsis-induced tight junction injury and vascular endothelial hyperpermeability *via* the Axl/NF-κB signaling pathway. *Front. Pharmacol.* **10**, 662 (2019).
66. S. Y. Bae, J. Y. Hong, H. J. Lee, H. J. Park, S. K. Lee, Targeting the degradation of AXL receptor tyrosine kinase to overcome resistance in gefitinib-resistant non-small cell lung cancer. *Oncotarget* **6**, 10146–10160 (2015).
67. Y. Lu *et al.*, Regulated intramembrane proteolysis of the AXL receptor kinase generates an intracellular domain that localizes in the nucleus of cancer cells. *FASEB J.* **31**, 1382–1397 (2017).
68. A. T. Piala *et al.*, Chloride sensing by WNK1 involves inhibition of autophosphorylation. *Sci. Signal.* **7**, ra41 (2014).
69. R. Akella *et al.*, Osmosensing by WNK kinases. *Mol. Biol. Cell* **32**, 1614–1623 (2021).
70. H. Y. Shin, R. M. Underwood, M. W. Fannon, Fluid pressure is a magnitude-dependent modulator of early endothelial tubulogenic activity: Implications related to a potential tissue-engineering control parameter. *Tissue Eng. Part A* **18**, 2590–2600 (2012).
71. P. Zhang *et al.*, Osmotic stress, not aldose reductase activity, directly induces growth factors and MAPK signaling changes during sugar cataract formation. *Exp. Eye Res.* **101**, 36–43 (2012).
72. C. Bellomo, L. Caja, A. Moustakas, Transforming growth factor β as regulator of cancer stemness and metastasis. *Br. J. Cancer* **115**, 761–769 (2016).
73. T. Nakagawa *et al.*, TGF-beta induces proangiogenic and antiangiogenic factors via parallel but distinct Smad pathways. *Kidney Int.* **66**, 605–613 (2004).
74. L. Attisano, J. L. Wrana, Signal transduction by the TGF-beta superfamily. *Science* **296**, 1646–1647 (2002).
75. P. Nowak-Sliwinska *et al.*, Consensus guidelines for the use and interpretation of angiogenesis assays. *Angiogenesis* **21**, 425–532 (2018).
76. C. A. Schneider, W. S. Rasband, K. W. Eliceiri, NIH Image to ImageJ: 25 years of image analysis. *Nat. Methods* **9**, 671–675 (2012).
77. D. R. Stirling *et al.*, CellProfiler 4: Improvements in speed, utility and usability. *BMC Bioinformatics* **22**, 433 (2021).
78. S. M. Meadows, L. A. Ratliff, M. K. Singh, J. A. Epstein, O. Cleaver, Resolution of defective dorsal aortae patterning in Sema3E-deficient mice occurs via angiogenic remodeling. *Dev. Dyn.* **242**, 580–590 (2013).
79. H. R. Chen, T. M. Yeh, In vitro assays for measuring endothelial permeability by transwells and electrical impedance systems. *Bio Protoc.* **7**, e2273 (2017).
80. Z. Gu, L. Gu, R. Eils, M. Schlesner, B. Brors, circlize Implements and enhances circular visualization in R. *Bioinformatics* **30**, 2811–2812 (2014).